Int J Comput Vis (2010) 86: 243–255
DOI 10.1007/s11263-008-0165-1

On the Apparent Transparency of a Motion Blurred Object

Extracting information from blurred smears

Vincenzo Caglioti · Alessandro Giusti

Received: 11 February 2008 / Accepted: 30 July 2008 / Published online: 2 October 2008

Abstract An object which moves during the exposure time results in a blurred smear in the image. We consider the smear as if it was the image of a semitransparent object, and we retrieve its alpha matte by means of known techniques. The alpha value at a pixel is meaningfully interpreted as the fraction of the exposure time during which the object projection overlapped that pixel.

Basing on this fact, our work highlights interesting qualitative and quantitative properties of the alpha matte, which can be used to derive constraints on the object's apparent contour, and its motion during the exposure time, from a single motion-blurred image; we also show that some of these properties hold on the original image.

The theory is validated with experimental results both on synthetic and real images, highlighting strengths and limitations; we point out a range of possible applications, including blurred image interpretation, temporal superresolution of object contours, model-based reconstruction of nontrivial motion, and improvements of alpha matting techniques.

Keywords Motion blur · Alpha matting · Temporal superresolution · Finite exposure time

1 Introduction

When a moving object is photographed by a still camera, its image is motion blurred because the object's projection on the image plane changes during the exposure time (see Fig. 1). If the exposure time is not short enough in relation to the apparent motion speed, the object results in a visible, semitransparent "smear" or "streak" in the image, and its contours blend with the background confusing traditional computer vision techniques.

In this paper we work on a single image by analyzing the smear's alpha matte (i.e. its transparency), which can be recovered either by means an alpha matting algorithm, or when shooting in controlled conditions; we prove that the

Fig. 1 Motion blurred object images

V. Caglioti · A. Giusti (✉)
Dipartimento di Elettronica e Informazione, Politecnico di Milano, P.za Leonardo da Vinci, 32 20133, Milano, Italy
e-mail: alessandro.giusti@polimi.it

V. Caglioti
e-mail: vincenzo.caglioti@polimi.it

alpha matte of the blurred object image enjoys several interesting properties, which are linked to the object's apparent contour and its motion during the exposure time. Other than generically supporting the understanding of the object smear, this allows us to retrieve:

- the apparent contour at the beginning and end of the exposure;
- parts of the contour at arbitrary time instants inside the exposure time;
- envelopes of the moving contour;
- the path of corners on the contour;
- speed discontinuities of the contour, caused for example by impacts of the moving object.

In Sect. 5.2 we also show that, in simple scenes, some of this information can directly be recovered on the original image, without alpha matting.

In general, the interpretation of motion blurred object images may be useful for the analysis or enhanced visualization of an existing image; but we also maintain that, in some situations, a vision system may provide motion-blurred images by design from which additional information can be recovered. For example, longer exposure times may be used to reduce noise, or object motion may be too fast for acquiring sharp images; also, applications dealing with known objects may use a lower frame-rate while increasing image resolution, or even use an ordinary camera instead of a video camera; information from motion blur is also insensitive to temporal aliasing issues and does not require to solve the correspondence problem. Moreover, some of our results on the alpha matte structure may be exploited for improving alpha matting algorithms. Section 5.3 provides an overview and examples of some of these applications.

The paper is structured as follows: after providing an overview of related works (Sect. 2), we recall a general model for motion-blurred image formation (Sect. 3), and show how the smear's transparency can be meaningfully interpreted in this context; we briefly show how transparency can be recovered under varying constraints, then introduce our notation and basic properties. In Sect. 4 we present our main results, which relate features on the alpha matte to meaningful constraints on the moving object's apparent contours during the exposure time. We discuss practical issues and applications of our theory in Sect. 5, whereas Sect. 6 presents experimental results on both real and synthetic images. Finally, we provide conclusions and list future works (Sect. 7).

2 Related Works

Most literature dealing with motion blur is concerned with removing it ("deblurring"), either assuming that it affects the whole image because of camera shake (Fergus et al. 2006; Slepian 1967), or aiming at deblurring moving objects (Kang et al. 1999). Interestingly, in Jia (2007) the analysis of the blurred object's alpha matte is used as an aid for recovering the point spread function, with the goal of improving deblurring performance; the main advantage in using the alpha matte in that context lies in its deep relation to apparent motion during the exposure time; in the present paper we are exploring the details of such a relation.

Our approach also differs from deblurring-related works as our main aim is to extract the additional information that a single motion blurred image incorporates about the scene structure and evolution; such information is not available in a sharp image.

This idea is not new: back in 1996 (Chen et al. 1996) proposes to estimate apparent motion in the image by exploiting motion-blur cues. More recently, (Lin 2005; Lin and Chang 2005) exploit motion-blurred images in order to estimate the speed of a moving vehicle and of a moving ball, respectively; in Klein and Drummond (2005), rotational blur estimation is the basis for a visual gyroscope, and (Lin and Chang 2006) exploits motion blur to obtain depth information from a single blurred image. These approaches assume a specific blur model (linear or rotational) and compute results basing on its parameters. A more powerful approach to a similar, specific problem is proposed in Boracchi et al. (2007a, 2007b) which can be considered particular applications of the general theory we are presently describing: they are recalled in Figs. 11 and 12.

In Favaro and Soatto (2004) motion blur cues extracted from multiple images are used for joint reconstruction of geometry and photometry of scenes with multiple moving objects; in order to determine a motion estimate, which is needed both for deblurring and reconstruction, multiple images are used. On the contrary, in the present paper we explore the relationship between apparent transparency and object motion in a single image.

Instead of referring to a specific application, our work has a general validity when moving objects are imaged from a still camera, and provides a sound theoretical foundation for interpreting and extracting information from blurred smears; we use a general blur model, and do not require that blur is representable in the frequency domain. This allows us to handle any type of motion. Preliminary results of this work have been published in Giusti and Caglioti (2007b).

3 Model and Definitions

We begin by presenting a model for the image of a moving object, highlighting the connections to the matting problem by introducing the $\alpha(p)$ quantity, which will be our main object of study in the following.

3.1 Motion Blur Model and Its Relation with Alpha Matting

A motion blurred image is obtained when the scene projection on the image plane changes during the camera exposure period $[t', t'']$. The resulting image C is the integration of an infinite number of sharp images, each exposed for an infinitesimal portion of $[t', t'']$. In an equivalent interpretation (Fig. 2), we can consider the motion blurred image as the temporal average of an infinite number of still images I_t, each taken with the same exposure time $t'' - t'$ but representing the scene frozen at a different instant $t \in [t', t'']$. This technique is also implemented in many 3D rendering packages for accurate (but computationally expensive) synthesis of motion blurred images.

If the camera is static and a single object is moving in the scene, the static background in the final image is sharp since its pixels are of constant intensity in each I_t; conversely, the image pixels which are affected by the moving object, possibly only in some of the I_t images, belong to the motion-blurred image (smear) of the object.

For a pixel p, define $i(p) \subseteq [t', t'']$ the set of time instants during which p belongs to the object image. We finally define $\alpha(p)$ as the fraction of $[t', t'']$ during which the object projects to p:

$$\alpha(p) = \|i(p)\|/(t'' - t'). \tag{1}$$

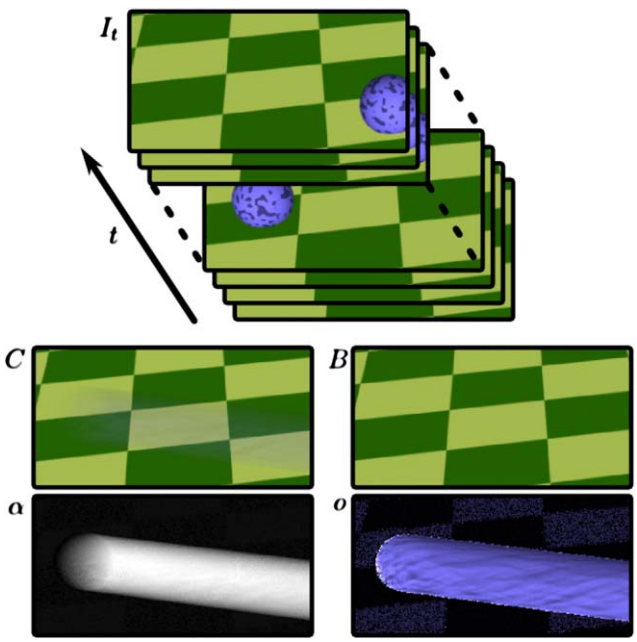

Fig. 2 Original image (C), background (B), transparency (α, rescaled for display purposes), foreground map (o). The image C of the motion blurred object can be interpreted as the temporal average over the exposure time of an infinite number of still images I_t (*top*). The blurred smear can be interpreted as a semitransparent layer, whose alpha matte (transparency) we analyze in the following

Let $B(p)$ be the intensity of the background at p. Since C is the temporal average of all the I_t images, $C(p) = \alpha(p)o(p) + (1 - \alpha(p))B(p)$. $o(p)$ is the temporal average over $i(p)$ of the intensity of image pixel $C(p)$:

$$o(p) = \frac{1}{\|i(p)\|} \int_{t \in i(p)} I_t(p)\, dt. \tag{2}$$

In short, the intensity of a pixel p in the motion blurred image C can be interpreted as the convex linear combination of two factors: the "object" intensity $o(p)$, weighted $\alpha(p)$, and the background intensity. The resulting equation is the well-known Porter-Duff alpha compositing equation (Porter and Duff 1984) for a pixel with transparency $\alpha(p)$ and intensity $o(p)$ over the background pixel $B(p)$. Recovering $\alpha(p)$ from a motion-blurred image is therefore equivalent to the well-known *alpha matting* (or *layer extraction*) problem.

In this context, the object intensity $o(p)$ can be interpreted as the intensity that p would have in the motion blurred image over a black background, rescaled by a $\frac{1}{\alpha(p)}$ factor. $o(p)$ is meaningless if p is not influenced by the object image during the exposure.

3.2 Recovery of the Alpha Matte

In the general case, the alpha matting problem is under-constrained, even if the background is known; however, the problem is crucial to many important computer graphics applications because even opaque objects with sharp apparent contours always have some *mixed pixels* (i.e. pixels where $0 < \alpha < 1$) at least around their contour; a correct alpha matting then allows one to obtain a faithful separation of the object and background. Mixed pixels also greatly increase in number when the object is defocused, motion blurred or semitransparent.

Therefore, many sophisticated algorithms have been proposed for extracting an object's alpha matte from an image, with varied performance and operating assumptions: some (Mishima 1993; Smith and Blinn 1999) require a specific background (*blue* or *green screen matting*), whereas others (Apostoloff and Fitzgibbon 2004; Berman et al. 2000; Chuang et al. 2001; Levin et al. 2006; Ruzon and Tomasi 2000; Sun et al. 2004), with minimal user assistance, handle unknown backgrounds (*natural image matting*) and possibly large zones of mixed pixels.

Although none of these algorithms is explicitly designed for the interpretation of blurred smears, as we show in Section 6 we can often get satisfactory results even with *natural image matting* algorithms, provided that a large enough area with $\alpha = 1$ is visible; on the contrary, in scenes with long blurred smears, densely-textured backgrounds, or poor foreground/background chromatic separation, *natural image matting* is seldom satisfactory.

As a first alternative, in more controlled settings which are common in many machine vision applications or when dealing with images of simple objects, other approaches can be used to pull the alpha matte of a severely motion-blurred object, possibly appearing very transparent everywhere. For example, if the object appears with a given constant intensity on a known background, $\alpha(p)$ can be readily derived at each pixel by solving a first-degree linear equation. In a color image, we can extend our considerations to all channels separately, noting that $\alpha(p)$ is constant along all the channels. Then, if the background is known and the object colors meet some constraints, $\alpha(p)$ can analytically be computed in the whole image (Giusti and Caglioti 2007a).

Moreover, as we discuss in Sect. 5.2, some of our results also hold for the original image; this is extremely useful in practice, because it provides a way to apply our theory even in situations where alpha matting is infeasible, unreliable or too computationally intensive.

3.3 Basic Definitions

During the exposure time $[t', t'']$, the object contour changes. Let $c(t)$ be the object apparent contour at t.

We partition the image into regions, which we classify on the basis of two criteria:

- Whether the points in the region are inside $c(t')$ ($R^\bullet$) or not (R°), which we indicate with a superscript.
- How many times each image point belonging to the region is crossed by c during the exposure time, which we indicate with a subscript.

The background ($\alpha(p) = 0$) is the R_0° region. On the contrary, the $R_0^\bullet$ region is composed by all and only the pixels covered by the object during the whole exposure ($\alpha = 1$); in the example in Fig. 3, there is no $R_0^\bullet$ region.

Note that if any point inside $c(t')$ is crossed once by the apparent contour, it will be outside $c(t'')$, and vice-versa; this is easily generalized to the following property.

Property 1 An $R_{2n+1}^\bullet$ or R_{2n}° region is outside $c(t'')$. An $R_{2n}^\bullet$ or R_{2n+1}° region is inside $c(t'')$.

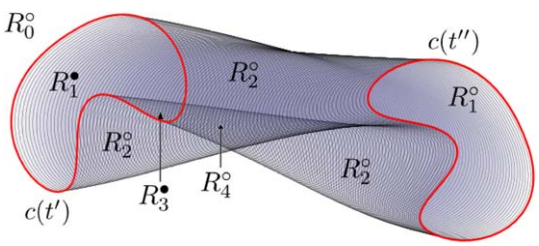

Fig. 3 The smear of a rotating bean-shaped object translating from left to right, and its regions

4 Properties of the Blurred Smear Alpha Matte

In this section the main contributions of the paper are shown. We present a meaningful property of α values in R_1 regions, then discuss region topology, classify borders between regions, and give meaningful physical interpretations of such borders. Finally, we show how region borders relate to features which can be detected in the alpha matte.

4.1 α Inside R_1 Regions

As we just introduced, R_1 regions are crossed by the object's apparent contour only once during the exposure time. This allows us to derive the following theorem, which enables applications such as temporal superresolution of object contours (see Sect. 5.3).

Theorem 1 *The iso-α curve $\alpha = \bar{\alpha}$ within an $R_1^\bullet$ region is part of the apparent contour $c(t' + \bar{\alpha}(t'' - t'))$. Similarly, the iso-$\alpha$ curve $\alpha = \bar{\alpha}$ within an R_1° region is part of $c(t'' - \bar{\alpha}(t'' - t'))$.*

Proof Each pixel p belongs to the object image for exactly $\alpha(p)(t'' - t')$ seconds. In an $R_1^\bullet$ region each pixel is crossed once by the object contour, therefore it belongs to the object image during a compact time interval starting at t' and ending when it is crossed by the object contour, at time $t' + \alpha(p)(t'' - t')$. The first part of the thesis immediately follows. A similar argument holds for the second part of the thesis. □

Corollary 1 *In an R_1 region the direction of $\nabla\alpha(p)$ is orthogonal to the object contour in p at time $\alpha(p)(t'' - t')$; $|\nabla\alpha(p)|$ is inversely proportional to the apparent contour motion speed component along the direction of $\nabla\alpha(p)$. In an R_1° region $\nabla\alpha(p)$ points towards the motion direction, whereas in $R_1^\bullet$, $\nabla\alpha(p)$ points towards the opposite direction.*

4.2 Region Borders

Other than α values inside R_1 regions, another important source of information in the object smear is represented by borders between regions.

Definition 1 We classify borders between regions as follows:

type 1a: separates an R_n region from an R_{n+1} region, inverting the superscript;
type 1b: separates an R_n region from an R_{n+1} region, preserving the superscript;
type 2: separates an R_n region from an R_{n+2} region, always preserving the superscript.

Theorem 2 *Under broad assumptions, detailed in Sect.* A.3:

i *All possible borders between regions can be classified according to Definition* 1; *multiple borders may overlap at isolated points.*
ii *The union set of all type* 1a *borders coincides with* $c(t')$; *the union set of all type* 1b *borders coincides with* $c(t'')$.
iii *A type* 2 *border is the envelope*[1] *of* $c(t)|_{t\in[t1,t2]\subseteq[t',t'']}$;

Proof See Appendix A.3. □

The theorem follows from the intuitive observation that region boundaries only occur at $c(t')$, $c(t'')$ and at envelopes of the object's apparent contour (see Fig. 3).

The theorem shows that region boundaries summarize meaningful information about the scene evolution during the exposure time; this is especially significant in practice because, as we are going to introduce, region boundaries can often be detected from the alpha matte (or even directly from the original image, as described in Sect. 5.2).

4.3 Interpretation of features on the alpha matte

Theorem 3 *Under broad assumptions, detailed in Appendix* A.4, *let* $\nabla\alpha$ *be the gradient of* α; *if* p *belongs to a region border then* $\nabla\alpha$ *is discontinuous in* p.

A proof sketch is provided in Appendix A.4; the theorem follows from the interpretation of α given in (1).

Remark 1 The reverse of Theorem 3 does not normally hold; it holds if the apparent contours are smooth, strictly convex, and move with continuity in speed; these are very restrictive assumptions, which are met e.g. by the perspective image of a strictly convex smooth solid in free motion. Then, $\nabla\alpha$ has a jump discontinuity always and only across a region border. In particular, at a type 1 border $\nabla\alpha$ has a jump discontinuity whose both left and right limits have finite norm. At a type 2 border, one of the left or right limits of $\nabla\alpha$ has infinite norm.

In the general case, instead, we easily derive from the proof of Theorem 3 that, in addition to region boundaries, any abrupt change in the speed or orientation of (a part of) the apparent contour results in a discontinuity in $\nabla\alpha$. This occurs:

- along the path of a corner on the apparent contour;
- when the object suddenly changes its motion at a time $\bar{t}$, e.g. as the result of an impact; in this case a discontinuity in $\nabla\alpha$ overlapping with $c(\bar{t})$ is originated;
- when the moving object is not strictly convex: then a discontinuity in $\nabla\alpha$ at point p occurs as p's viewing ray is bitangent to the object at a given $t \in [t', t'']$.

[1] If $c(t)$ is not smooth, (part of) a type 2 border may represent the locus of points touched by a corner displacing along a direction not included by the corner itself. This slightly broadens the definition of envelope.

5 Discussion and Practical Considerations

5.1 Classifying Borders and Regions

Theorem 3 allows us to locate a superset of all region borders by looking for discontinuities in $\nabla\alpha$. Type 2 borders, when representing the envelope of smooth contours, are easily classified because $\nabla\alpha$ has an extremely large norm just besides the border.

Only if the restrictive assumptions in Remark 1 hold, which ensure the validity of the reverse of Theorem 3, then there is a one-to-one relation between discontinuities and borders. Else, some discontinuities may be spurious, and e.g. may represent the path of corners in the apparent contour which do not originate a legitimate region border, or outline the contour when the object abruptly changes its speed. In some applications (see Fig. 5 row 2 and Fig. 12), one may take advantage of such information.

R_0° and $R_0^\bullet$ regions can be initialized where $\alpha = 0$ and $\alpha = 1$, respectively.

The type 1 borders constitute the union of $c(t')$ and $c(t'')$. Assuming that the two can be separated, there is an ineliminable ambiguity about which is which, so one is arbitrarily chosen as $c(t')$ and classified as Type 1a; all contained regions are set as $R^\bullet$; all remaining regions are R°.

As a result of such ineliminable ambiguity, *two consistent region labellings always exist, corresponding to opposite motion directions of the object*; one can be transformed into the other by simply inverting the superscript of odd regions (see Fig. 4). This is linked to the fact that the orientation of apparent motion cannot be recovered by a blurred image: in fact, as the blurred image is modeled as the sum of many sharp images (see Sect. 3), the order of such images is lost.

Instead, the region subscripts (indicating the number of times each point is crossed by the apparent contour during the exposure time) are not affected by the ambiguity, and can be derived by means of the constraints stated in Definition 1; we verified on synthetic images that, assuming a correct classification of type 1 and type 2 borders, in most cases only one consistent labeling (plus its "inverted" twin) satisfies all such constraints. However, counterexamples can be found, where more than one consistent region labeling (plus the respective "inverted" twins) exists; trivially, this

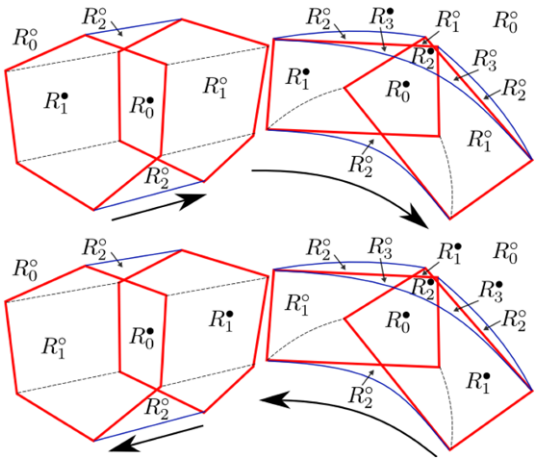

Fig. 4 (Color online) Interpretation of cube (second row of Fig. 6) and business card (first row of Fig. 7) smears. *Blue lines*: type 2 region borders; *thick red lines*: type 1 region borders; *thin dashed lines*: paths of corners on the apparent contour (*not* a region border). For each scene, the two twin labellings associated to opposite motion directions are given; in this case, assuming type 1 and type 2 borders are correctly identified, they are the only two consistent labellings (see Sect. 5.1)

happens every time more than one independent blurred object is shown. In practice, also in scenarios where region borders are not known in detail, such as in some of the examples of Fig. 9, ambiguities must be accepted; this is better illustrated in the supplementary material videos (Supplementary material 2008).

Automatic identification and labeling of regions (up to the ineliminable ambiguity cited above) is possible in simple scenes, or where additional information about the scene is known (see example in Fig. 11).

5.2 Operating on the Original Image

Under broad assumptions, discontinuities in $\nabla\alpha$ result in discontinuities in the gradient of the original image. Locating region borders and other features directly from the image gradient is therefore possible in several practical scenarios, without the need of alpha matting, as demonstrated in Figs. 5, 10 and 11. Depending on the application, actual feasibility may be hindered by the interference of the background and object texture and shading, which obviously generate additional discontinuities in the image gradient. Still, we point out that discontinuities due to the path of corners or envelopes in the object texture may provide useful information, as in the example in Fig. 12.

5.3 Applications

By locating and classifying regions, their borders, and other discontinuities of $\nabla\alpha$, strong constraints on the object apparent contours during the exposure can be found. This allows one to extract a wealth of motion information from the object smear, which would not be available in a sharp image.

5.3.1 *Re-animating a Blurred Smear*

Independently on the specific application scenario, Theorem 1 allows one to partially reconstruct apparent contours at intermediate time instants belonging to the exposure period, as the union set of an iso-α curve with value $\bar{\alpha}$ within $R_1^\bullet$ and an iso-α curve with value $1-\bar{\alpha}$ within R_1°. Examples of this possibility—which requires the knowledge of the object's alpha—are shown in Figs. 6, 7 and 9, and in the supplementary material (Supplementary material 2008).

Our prototype requires user interaction in form of scribbles for alpha matting (black/white in Fig. 8), and scribbles for discriminating R_1° and $R_1^\bullet$ regions (red/blue in Fig. 8). Further automation of the procedure may also be possible in the future:

- scribbles for matting may be avoided by exploiting that the foreground itself is blurred; techniques such as (Favaro and Soatto 2004) may provide a first automatic segmentation to be fed to the matting algorithm;
- R_1 regions may be automatically detected in scenes depicting simple motions by means of simple heuristics, as they are usually the biggest regions where $0<\alpha<1$. On the other hand, discriminating R_1° from $R_1^\bullet$ regions is often a difficult task which may require interpreting the scene semantics. This is especially true when there are many R_1 regions and where region boundaries are not well defined. Also, the ineliminable ambiguity between the two consistent labellings mentioned in Sect. 5.1 is always present.

Reconstructed contours can be visualized as lines superimposed to the image; alternatively, a better-looking video (see supplementary material (Supplementary material 2008)) can be synthesized by copying background or foreground pixels in appropriate parts of the R_1 regions. In particular, a frame I_t at time $t\in\,]t',t''[$ can be generated from the original image C and the images returned by the matting algorithm: the alpha mask α, the foreground F and the background B. For each pixel p,

- if p does not belong to an R_1 region, $I_t(p)=C(p)$;
- if p belongs to an $R_1^\bullet$ region:
  - if $(t-t')/(t''-t')<\alpha(p)$, then $I_t(p)=F(p)$;
  - else $I_t(p)=B(p)$
- if p belongs to an R_1° region:
  - if $(t-t')/(t''-t')<\alpha(p)$, then $I_t(p)=B(p)$;
  - else $I_t(p)=F(p)$

In the future, instead of just copying the blurred foreground, deblurring algorithms may be selectively applied on the foreground for showing the sharp object in motion. However, the problem is not straightforward as such blur is space-variant.

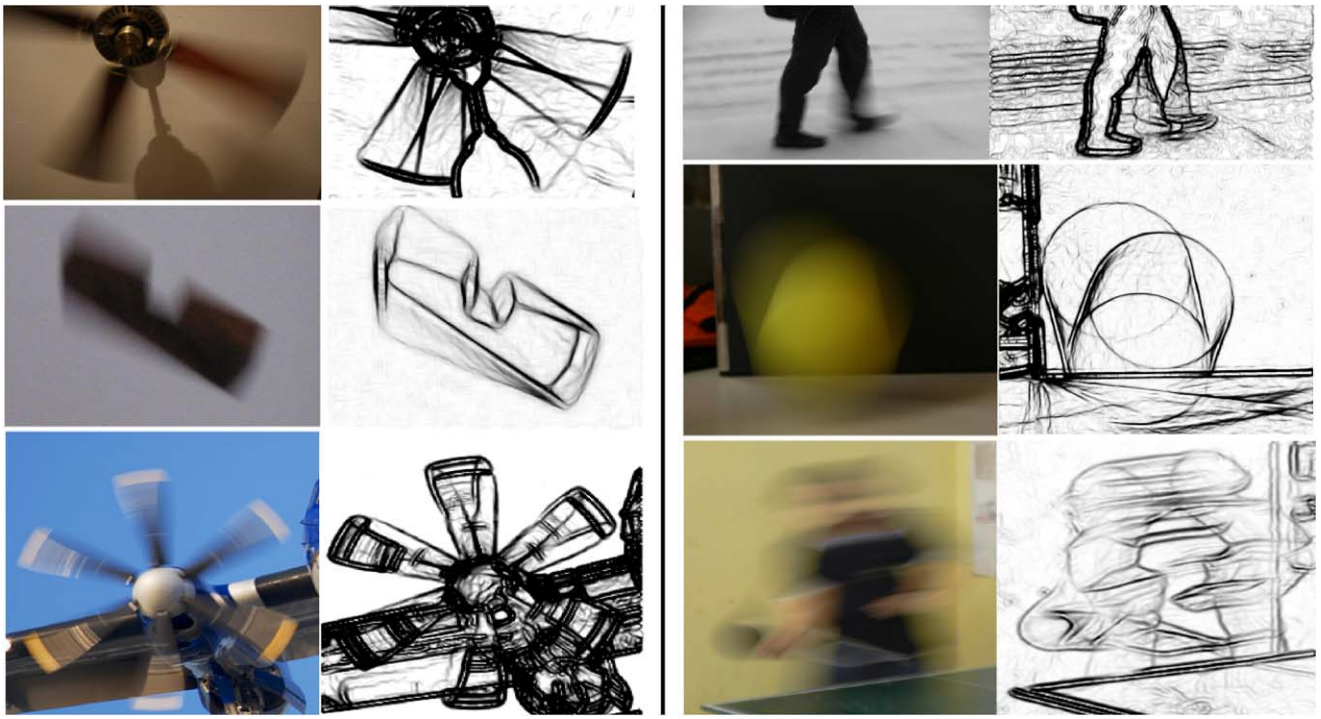

Fig. 5 Original image (*left*), and discontinuities computed directly over its gradient, without recovering α (*right*). As explained in Sect. 4.3, you can see the objects' contours at the beginning and end of the exposure, as well as, in the *second row on the right*, the ball's contour at the bounce position (sudden speed discontinuity). In most of these images, the alpha matte cannot be reliably extracted with known algorithms, mostly due to the limited size of the $R_0^\bullet$ region; therefore, we cannot extract the evolution of contours during the exposure time

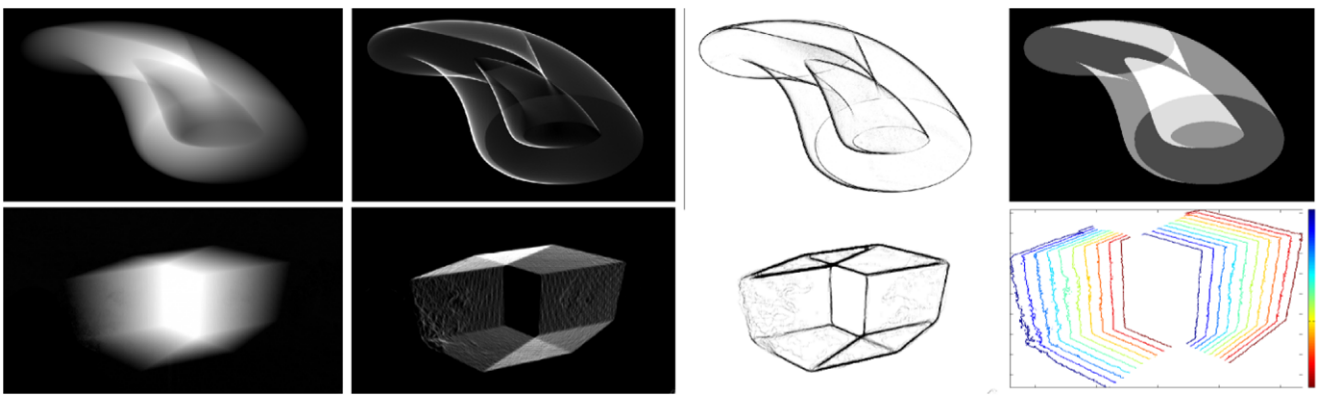

Fig. 6 Results on synthetic images. *First row*: rototranslating torus; *from left to right*: α; $|\nabla\alpha|$; discontinuity in $\nabla\alpha$ (see text); ground truth region subscripts, 0 (black) to 5 (white). *Second row*: translating cube; rightmost image represents part of $c(t)$ at intermediate, equally-spaced instants during the exposure, reconstructed as iso-alpha curves (Theorem 1). See supplementary material (Supplementary material 2008) for details

5.3.2 *Temporal Superresolution of Videos*

A similar application can also be used for temporal superresolution of apparent contours in a video whose frames are exposed for a significant part of the inter-frame interval; this has analogies with Shechtman and Caspi (2005), which tackles a similar problem with a completely different approach: they exploit multiple videos of the same dynamic scene, whose exposure periods are not overlapping, which allows them to reconstruct a video with an higher frame rate. Another sophisticated application of the same principle could consist in partial 3D reconstruction of a rototranslating object from a single image (e.g. using a standard multiview approach such as Furukawa et al. 2006).

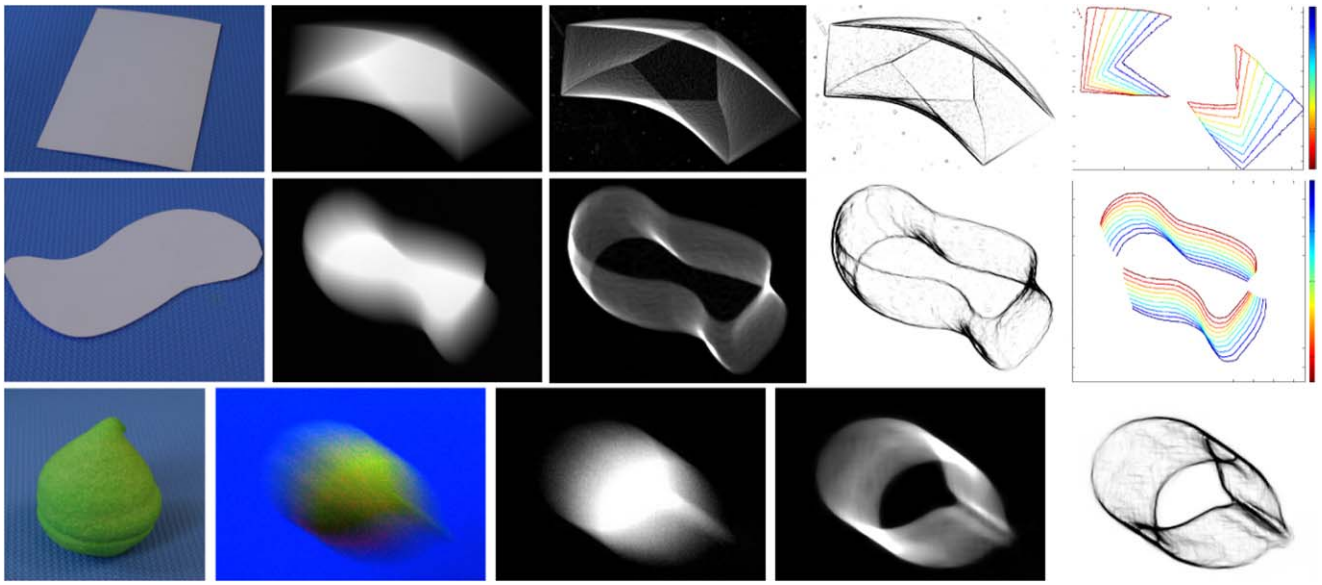

Fig. 7 Results on real images, controlled conditions. *First row*: white rectangular business card moving on a dark desk; *from left to right*: the object; the blurred image (from which α follows immediately); $|\nabla\alpha|$; discontinuity in $\nabla\alpha$; contour motion as iso-alpha curves. *Second row*: A planar object with curvy contours moving on a dark desk. *Third row*: A candy. Second image is the actual blurred image (exposure time 20 ms): note severe shading and noise. Alpha (*third image*) is computed using Levin's matting algorithm. See supplementary material (Supplementary material 2008) for reconstructed videos in the three cases

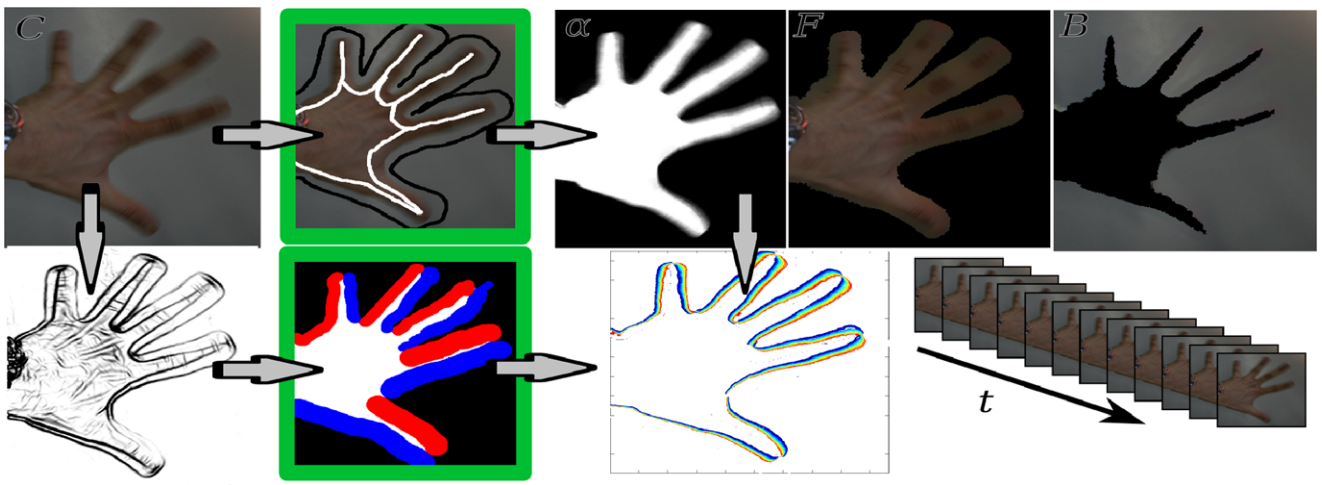

Fig. 8 Steps for re-animating a blurred smear. *First row* shows alpha matting. Images in rounded thick borders are user scribbles

5.3.3 *Other Applications*

Theorem 2 allows us to identify $c(t')$ and $c(t'')$, which is a valuable information in many practical applications; in Fig. 11, we exploit this in order to reconstruct the 3D position *and velocity* of a moving ball from a single slightly blurred perspective image; Figs. 5 and 10 also show related examples.

Information about contour envelopes and corner paths can also be valuable for reconstructing motion in simple scenes, which has applications in machine vision or for understanding high-speed dynamic events with the high resolution and low price of an ordinary digital camera (see Fig. 12).

6 Experimental Results

The theoretical results we presented in the previous sections have been validated by experimental results both on real (Figs. 5 and 7 to 12) and synthetic (Fig. 6) images.

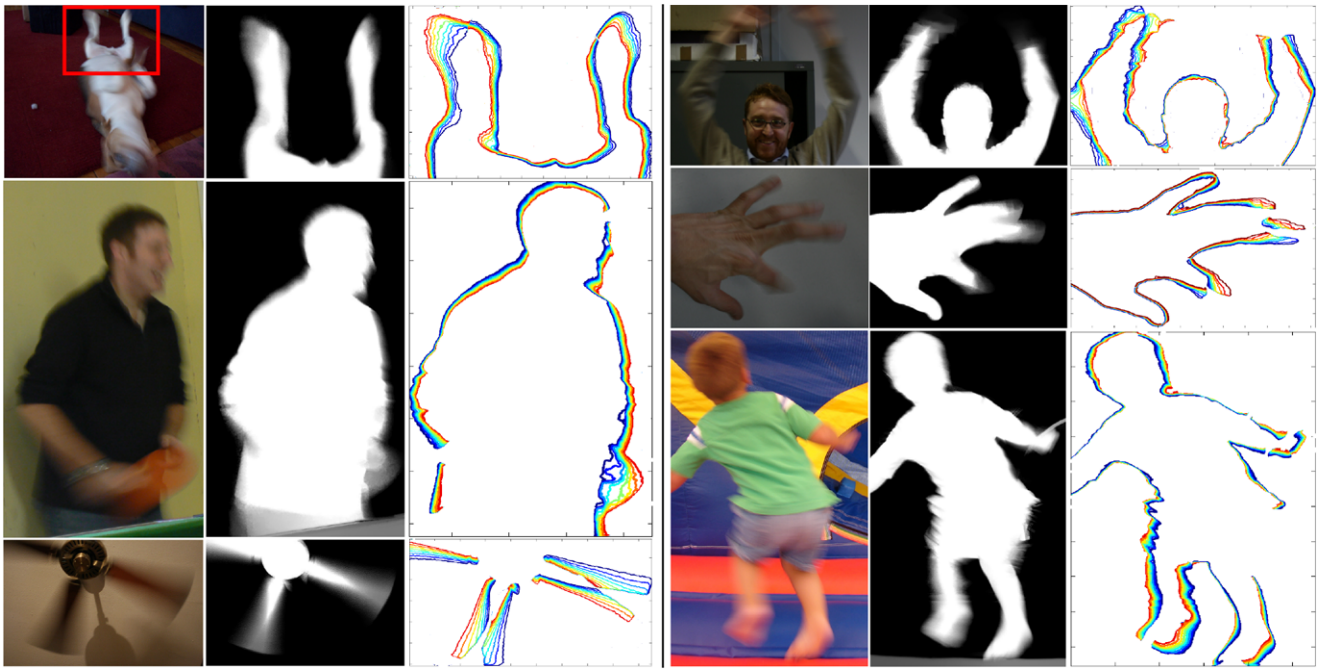

Fig. 9 Application to temporal superresolution of object contours using alpha matting. *First column*: original image; *second column*: alpha matte found by (Levin et al. 2006); *third column*: evolution of contours during exposure time. The procedure is detailed in Sect. 5.3.1 and Fig. 8. See supplementary material (Supplementary material 2008) for videos of reconstructed motion in these and other scenes. In some scenes, several consistent labellings are possible

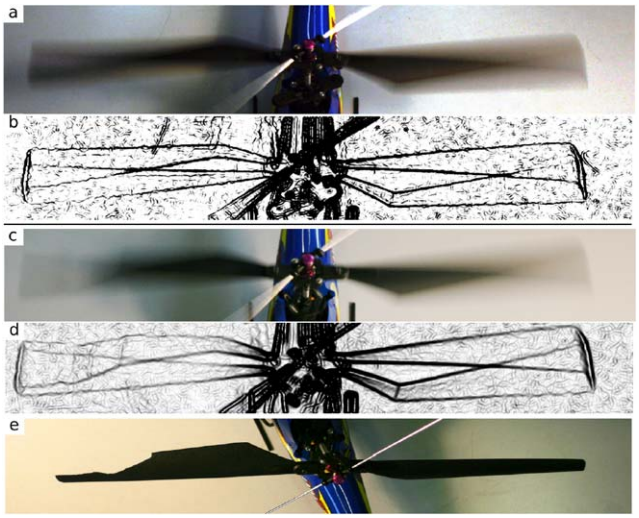

Fig. 10 **a**, **c**: Rotating blades of a radio controlled model helicopter imaged from above with an exposure time $= 1/50s$; **b**, **d**: discontinuities in $\nabla\alpha$; note visible shape of blades; note that angular speed measurement insensitive to temporal aliasing is possible; **e**: still shot of scene **c**: broken blade shape is visible in **d**

6.1 Synthetic Images

Synthetic images were generated using the popular Blender raytracing software, by creating an animation with several hundred frames and averaging them to obtain the actual motion-blurred image. Knowledge of the single frames also allows us to automatically compute the ground truth for the region labeling, as in top right of Fig. 6. We extracted alpha data by means of the technique in (Giusti and Caglioti 2007a), and verified that the result exactly matches the true alpha, generated by rendering the object in each frame as plain white on a plain black background.

6.2 Camera images

We also verified our techniques on real images. Some have been shot in a controlled environment (Fig. 7), using a digital reflex camera which allows us to manually control of exposure time, and using RAW images in order to avoid non-linearities in the camera response function; we both imaged uniform-color objects on an uniform background (which trivially translates to alpha data, possibly up to a scale factor if no $\alpha = 1$ region is visible), and objects meeting the color constraints in (Giusti and Caglioti 2007a) over a known background.

Moreover, we also show results on generic photographs and video frames shot by a variety of inexpensive digital cameras and camcorders; where a sufficiently extended $R_0^\bullet$ region was visible, we extracted α by means of the natural image matting algorithm by Levin et al. (2006), which interestingly returned acceptable results in this unforeseen setting (Fig. 9).

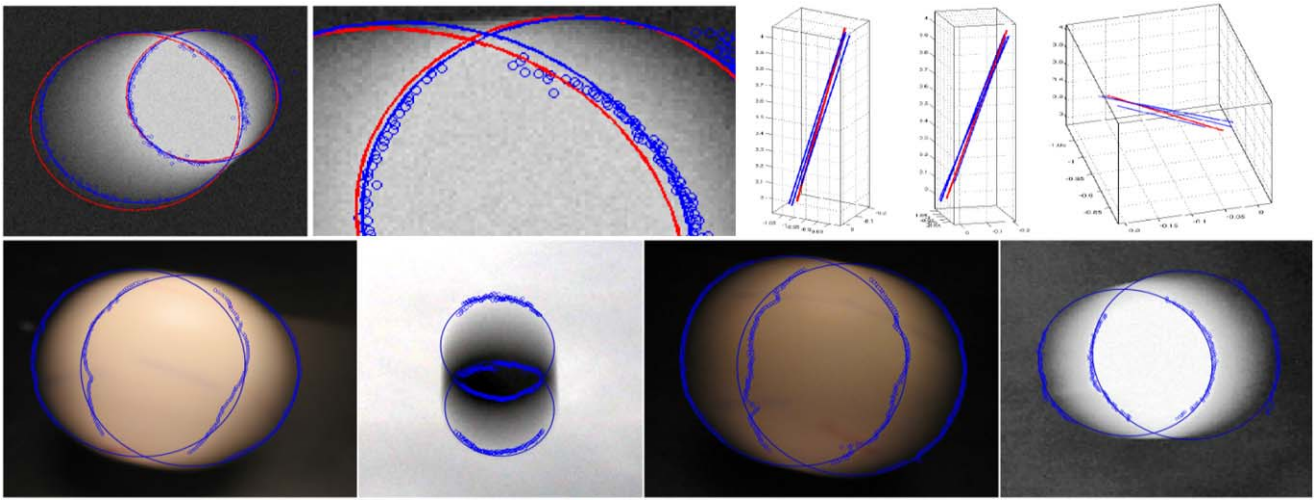

Fig. 11 (Color online) An application of our theory to fully-automated 3D localization of a moving ball from a single perspective image (Boracchi et al. 2007a). If the ball appears even slightly blurred, the traditional method of fitting an ellipse to its apparent contour does not work. We exploit Theorem 3, and look for angular points along rectilinear intensity profiles parallel to the ball's motion; these points lie on $c(t')$ and $c(t'')$; by fitting two ellipses on the two sets of points, we are able to reconstruct the 3D position *and velocity* of the moving ball from a single image. *Top row* shows a synthetic example (with added Gaussian noise): *blue dots* are discontinuities in the image intensity derivative along profiles, after denoising; *red ellipses* are the ground truth for $c(t')$ and $c(t'')$; blue ellipses are our estimate, obtained by fitting to blue dots; on the right, each 3D blue line represents our reconstructed position and velocity with a different realization of noise; *red line* is ground truth; other orientations of the same plot are also given. *Bottom row* shows the same algorithm on four different camera images (where ground truth is not available)

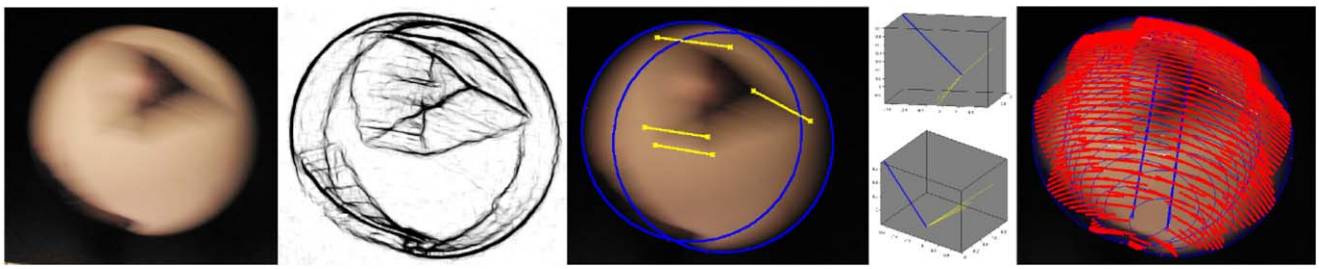

Fig. 12 (Color online) An application of our theory to user-assisted reconstruction of a blurred ball's 3D velocity, spin axis and angular speed from a single motion-blurred image. First image represents a blurred table tennis ball with a triangle drawn on its surface. First $c(t')$ and $c(t'')$ are automatically found as in Fig. 11; then the user selects the paths of corners in the ball texture (*third image*), which are well visible in the $\nabla\alpha$ discontinuity map (*second figure*); this allows us to apply the geometric technique in Boracchi et al. (2007b) for recovering the spin axis and angular speed. *Last image* shows reconstructed axis at the beginning and end of the exposure (*blue*) and motion of points on the ball surface (*red*)

6.3 Implementation Notes

As a measure of $\nabla\alpha$'s discontinuity, we computed the norm of the derivatives of $\nabla\alpha$ along the x and y directions, then combined them to a single measure, which we represent as black on white background in our figures; we applied some mild median and Gaussian filtering on $\nabla\alpha$ in order to mitigate the effect of noise, which is obviously amplified by the double differentiation. We also found that applying state-of-the-art discontinuity-preserving denoising algorithms (Dabov et al. 2007; Foi et al. 2007) on the original images greatly improves visual results. It is worth noting that these results have been obtained by using naive techniques for finding discontinuities, as the use of more sophisticated techniques is beyond the scope of the paper, and possibly application-dependent. In Fig. 11 we provide an example of a specialized fully-automated technique applied to motion-blurred ball localization.

We mainly worked with low-resolution images (less than 1 megapixel), or with small crops of high-resolution images; we found that resolution is not a critical factor. On the other hand, noise creates severe problems to the detection of region borders (Figs. 5, 6, 7 and 10), but has only a limited impact on iso-alpha curves for temporal superresolution (Figs. 6, 7, and 9).

7 Conclusions and Future Works

We presented a number of techniques for analyzing motion-blurred object smears, and relate their features to the object apparent contour and its evolution during the exposure period.

We initially isolate the contribution of the actual object motion by extracting the alpha matte of the semitransparent smear. Discontinuities in $\nabla\alpha$ partition the image into regions. We classify each region by means of two orthogonal criteria:

- the number of times each point in the region is crossed by the apparent contour during the exposure;
- whether the region is inside the object contour when the exposure begins.

Inside the regions crossed once by the apparent contour, iso-alpha curves represent the object contours at intermediate times during the exposure.

The object contours at the beginning and the end of the exposure are visible as region borders. The envelope of the object apparent contour over time also originates a region border. Discontinuities in $\nabla\alpha$ not mapping to a region border are still informative, since they either represent the path of a corner in the apparent contour, or the contour of the object when a sudden change in its motion occurs.

Experimental results and application examples confirm the validity and utility of the theory we presented on both synthetic and real images. Our current and future work on the topic is aimed at:

- reducing user intervention and improving output quality in our software for automated synthesis of a short video from a single motion blurred image, as described in Sect. 5.3;
- developing an automated system for temporal superresolution of low frame rate video by exploiting state-of-the-art video matting and video denoising techniques;
- adapting existing matting algorithms for improved alpha matting of blurred smears, by exploiting the strong constraints on the alpha described in this paper; moreover, knowledge of the blur in the smear foreground may further facilitate the matting process.
- experimenting with the additional information multiple images of the same scene with partially overlapping exposure times may bring on the object motion.

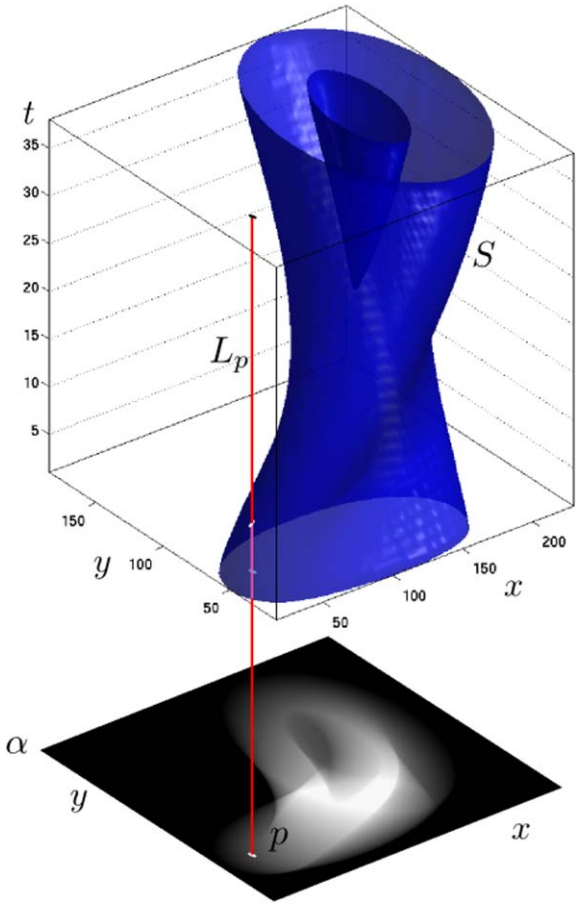

Fig. 13 Line L_p intersects S once, since p belongs to an R_1 region

Consider a 3D solid K in the (x, y, t) space, such that each cross section of K at $t = \bar{t}$ coincides with the image region inside $c(\bar{t})$. K is bounded by $t = t'$ and $t = t''$ planes, and summarizes the evolution of the object contours during the exposure.[2] We also refer to S (see Fig. 13), which is the lateral surface of K, i.e. the surface of K except the upper $(t = t')$ and lower $(t = t'')$ caps;[3] the intersection of S with a $t = \bar{t}$ plane is $c(\bar{t})$.

Consider a point $p = (p_x, p_y)$ on the x, y plane, and a line L_p in the x, y, t space, defined as $x = p_x$, $y = p_y$. The number of intersections of S with L_p coincides with the number of times image point p is crossed by c during the exposure time.

Appendix A

A.1 Space-Time Representation of $c(t)$

We now introduce a space-time representation of the contour evolution, which will be used in the following.

[2] Interestingly, a similar representation has been previously proposed for action classification Yilmaz and Shah (2005)

[3] S may be composed by several isolated parts (as in the figure), but we assume that each is smooth everywhere except possibly in a 0-measure set (ridge)

A.2 Degenerate Points

Definition 2 On the basis of the representation just introduced, we consider three conditions related to an image point p:

(a) p belongs to $c(t')$;
(b) p belongs to $c(t'')$;
(c) L_p is tangent to S at a single point;

Definition 3 An image point p is a degenerate point if and only if:

- L_p is tangent to S at multiple points; *or*,
- p satisfies more than one of the conditions in Definition 2.

Degenerate points are points belonging to more than a single region border; in the following, by assuming a discrete set of degenerate points, we exclude that two borders coincide along a finite curve.

In practice, this condition is always met except than in very special cases. Examples of violating scenes are an object moving with a trajectory which exactly retraces itself, or an object with a straight horizontal contour part translating horizontally (a segment of a type 1a border overlaps a part of a type 2 border).

However, even in scenes not meeting such constraints, most of the properties we show in this paper still hold with minor modifications and more convoluted proofs.

A.3 Details on Theorem 2

Theorem 2 holds if apparent contours move with finite speed and at most a discrete set of degenerate image points exists.

Under these assumptions (*Theorem 2*):

i All possible borders between regions can be classified according to definition 1; multiple borders may overlap at isolated points.
ii The union set of all type 1a borders coincides with $c(t')$; the union set of all type 1b borders coincides with $c(t'')$.
iii A type 2 border is the envelope[4] of $c(t)|_{t\in[t1,t2]\subseteq[t',t'']}$;

Proof of Theorem 2 Consider a non-degenerate image point p. Then we are in one of the following cases.

- None of the properties in Definition 2 holds. Then p is not part of a region border. In fact, all points p' in p's neighborhood belong to the same region as p, because:
  - their associated $L_{p'}$ lines in x, y, t space are crossed by S the same number of times, so the region subscript is kept;
  - points p' are either all inside or all outside $c(t')$, so the region superscript is kept.
- Only property (a) holds. Then p belongs to a type 1a border. In fact, in any neighborhood of p two points p' and p'' exist such that $L_{p'}$ crosses S k times, and $L_{p''}$ crosses S $k+1$ times. p' and p'' are at opposite sides of $c(t')$, thus the region superscript is inverted.
- Only property (b) holds. Then p belongs to a type 1b border. p' and p'' are not at opposite sides of $c(t')$, thus the region superscript is preserved.
- Only property (c) holds. Then p belongs to a type 2 border. In fact, in any neighborhood of p two points p' and p'' exist such that $L_{p'}$ crosses S k times, and $L_{p''}$ crosses S $k+2$ times. The region superscript is kept because all points in the neighborhood are either inside or outside $c(t')$.

□

A.4 Details on Theorem 3

Theorem 3 holds under the following assumptions:

- apparent contours move with finite speed and at most a discrete set of degenerate image points exists;
- absence of cusps on S;
- absence of a ridge on S whose projection on the x, y plane overlaps along a finite curve with a region border or with the projection of a different ridge;

Under these assumptions (*Theorem 3*):

let $\nabla\alpha$ be the gradient of α; if p belongs to a region border then $\nabla\alpha$ is discontinuous in p.

In practice, the degenerate cases in the assumptions almost never occur in practice; they are needed to exclude that a discontinuity in $\nabla\alpha$ is neutralized by a corresponding opposite source of discontinuity.

Proof sketch for Theorem 3 $\alpha(p)$ can be interpreted as the total length of L_p's intersection with K. When p crosses a border of type 1, L_p crosses a ridge on the surface of K, which reflects to a discontinuity in $\nabla\alpha$: our hypotheses exclude that the discontinuity may be canceled by another ridge in K. When p crosses a border of type 2, P is tangent to K's surface, which reflects to a discontinuity in $\nabla\alpha$ as well, unless S has a cusp in the tangency point, which is excluded by our hypotheses. □

[4] If $c(t)$ is not smooth, (part of) a type 2 border may represent the locus of points touched by a corner displacing along a direction not included by the corner itself. This slightly broadens the definition of envelope.

References

Supplementary material (2008). Download at http://home.dei.polimi.it/giusti/ijcv/.

Apostoloff, N. E., & Fitzgibbon, A. W. (2004) Bayesian video matting using learnt image priors. In *Proceedings of CVPR 2004*.

Berman, A., Vlahos, P., & Dadourian, A. (2000). *Comprehensive method for removing from an image the background surrounding a selected object* (U.S. Patent 6,134,345).

Boracchi, G., Caglioti, V., & Giusti, A. (2007a). Ball position and motion reconstruction from blur in a single perspective image. In *Proceedings of international conference on image analysis and processing (ICIAP) 2007*.

Boracchi, G., Caglioti, V., & Giusti, A. (2007b). Single-image 3D reconstruction of ball velocity and spin from motion blur. In *Proceedings of VISAPP 2007*.

Chen, W., Nandhakumar, N., & Martin, W. (1996). Image motion estimation from motion smear—a new computational model. *IEEE Transactions on Pattern Analysis and Machine Intelligence*, *18*, 412–425.

Chuang, Y., Curless, B., Salesin, D., & Szeliski, R. (2001). A Bayesian approach to digital matting. In *Proceedings of CVPR 2001*.

Dabov, K., Foi, A., Katkovnik, V., & Egiazarian, K. (2007). Image denoising by sparse 3D transform-domain collaborative filtering. *IEEE Transactions on Image Processing*, *16*(8), 2080–2095.

Favaro, P., & Soatto, S. (2004). A variational approach to scene reconstruction and image segmentation from motion-blur cues. In *Proceedings of CVPR 2004*.

Fergus, R., Singh, B., Hertzmann, A., Roweis, S. T., & Freeman, W. T. (2006). Removing camera shake from a single photograph. In *ACM SIGGRAPH 2006 papers*.

Foi, A., Katkovnik, V., & Egiazarian, K. (2007). Pointwise shape-adaptive dct for high-quality denoising and deblocking of grayscale and color images. *IEEE Transactions on Image Processing*, *16*(5), 1395–1411.

Furukawa, Y., Sethi, A., Ponce, J., & Kriegman, D. (2006). Robust structure and motion from outlines of smooth curved surfaces. *IEEE Transactions on Pattern Analysis and Machine Intelligence*, *28*(2), 302–315.

Giusti, A., & Caglioti, V. (2007a). Isolating motion and color in a motion blurred image. In *Proceedings of BMVC 2007*.

Giusti, A., & Caglioti, V. (2007b). On the apparent transparency of a motion blurred object. In *Proceedings of PACV 2007 workshop*.

Jia, J. (2007). Single image motion deblurring using transparency. In *Proceedings of CVPR 2007*.

Kang, S., Choung, Y., & Paik, J. (1999). Segmentation-based image restoration for multiple moving objects with different motions. In *Proceedings of international conference on image processing (ICIP) 1999*.

Klein, G., & Drummond, T. (2005). A single-frame visual gyroscope. In *Proceedings of BMVC 2005*.

Levin, A., Lischinski, D., & Weiss, Y. (2006). A closed form solution to natural image matting. In *Proceedings of CVPR 2006*.

Lin, H.-Y. (2005). Vehicle speed detection and identification from a single motion blurred image. In *Proceedings of IEEE workshop on applications of computer vision* (pp. 461–467).

Lin, H.-Y., & Chang, C.-H. (2005). Automatic speed measurements of spherical objects using an off-the-shelf digital camera. In *Proceedings of IEEE international conference on mechatronics* (pp. 66–71).

Lin, H.-Y., & Chang, C.-H. (2006). Depth recovery from motion blurred images. In *Proceedings of international conference on pattern recognition (ICPR) 2006* (Vol. 1, pp. 135–138).

Mishima, Y. (1993). *Soft edge chroma-key generation based upon hexoctahedral color space* (U.S. Patent 5,355,174).

Porter, T., & Duff, T. (1984). Compositing digital images. In *Computer graphics*.

Ruzon, M., & Tomasi, C. (2000). Alpha estimation in natural images. In *Proceedings of CVPR 2000*.

Shechtman, E., & Caspi, Y. (2005). Space-time super-resolution. *IEEE Transactions on Pattern Analysis and Machine Intelligence*, *27*(4), 531–545.

Slepian, D. (1967). Restoration of photographs blurred by image motion. *The Bell System Technical Journal*, *46*(10), 2353–2362.

Smith, A. R., & Blinn, J. F. (1999). Blue screen matting. In *SIGGRAPH '96: proceedings of the 23rd annual conference on computer graphics and interactive techniques* (pp. 259–268).

Sun, J., Jia, J., Tang, C.-K., & Shum, H.-Y. (2004). Poisson matting. In *ACM SIGGRAPH 2004 papers* (pp. 315–321).

Yilmaz, A., & Shah, M. (2005). Actions sketch: a novel action representation. In *Proceedings of CVPR 2005*